

Emergent Cosmological Geometry Across a Superfluid Phase Transition: Reconciling BAO and CMB Without Expansion

Adam M. Sheldrick

December 23, 2025

Abstract

Recent observational tensions between late-time and early-time cosmological probes, most notably between baryon acoustic oscillations (BAO) and the cosmic microwave background (CMB), are commonly interpreted as evidence for new expansion-era physics or modifications to dark energy. In this work, we demonstrate that these tensions instead arise from an implicit but unjustified assumption: that a single effective geometric redshift law applies uniformly across all cosmic epochs.

Within the framework of a ECSV cosmology, we show that late-time observables probe an emergent, low-energy geometric response of a condensed medium, while early-time observables probe a distinct, pre- or transitional-phase regime with fundamentally different stiffness and propagation properties. The CMB is reinterpreted not as a relic of universal expansion, but as radiation emitted at a phase boundary in the medium. This naturally explains the survival of the acoustic angular scale θ_* without requiring global expansion, inflation, or dark matter.

We present a unified phenomenological description that preserves the empirical success of BAO and supernovae at late times, while resolving their apparent inconsistency with the CMB at early times.

1 Introduction

ECSV (Emergent Condensate Superfluid Medium) treats the vacuum as an effectively superfluid, condensate-like medium with dynamical fields whose gradients and defects carry stress, transport, and energy. In this view, phenomena usually attributed to spacetime curvature and unseen matter arise instead from the medium's local response laws (pressure-like stresses, solenoidal flow, and defect/flux-tube dynamics), with "geometry" emerging as an effective description of propagation and clock/ruler behaviour. The goal is not to draw a web by assumption, but to show that simple, conservative medium dynamics can self-organise into node-filament-void structure and reproduce the main cosmological observables through falsifiable, scale-bridging mechanisms.

The standard cosmological model assumes that a single spacetime metric, characterized by global expansion, governs the propagation of light across all epochs of the universe. Within this framework, the cosmic microwave background (CMB) is interpreted as a relic surface of last scattering, while baryon acoustic oscillations (BAO) and Type Ia supernovae are treated as late-time geometric probes of the same expanding background.

However, increasing observational precision has revealed persistent tensions between early-time and late-time measurements, particularly in the inferred sound horizon scale and Hubble parameter. These discrepancies are typically addressed by introducing additional early-universe components, modified expansion histories, or new dark sector physics.

In this paper, we take a fundamentally different approach. We argue that the tension itself is evidence that the assumption of a single, epoch-independent geometric redshift law is invalid.

This paper upgrades the earlier diagnostic proxy for weak lensing to an explicit ray-propagation calculation. The proxy is retained only as a qualitative guide; all quantitative conclusions in this work are based on direct numerical evaluation of the induction-path ray equation.

Scope and methodology. This paper upgrades the earlier diagnostic weak-lensing proxy to an explicit ray-propagation calculation. The proxy is retained only as a qualitative guide; all quantitative results presented here are based on direct numerical evaluation of the induction-path ray equation.

Interpretive Convention and Terminology

For clarity and ease of comparison with the observational literature, we employ standard cosmological notation (e.g. redshift z , high- z /low- z , distance–redshift relations) throughout this work. However, these symbols are used strictly as observational labels and do not imply an underlying expanding metric or a global scale factor $a(t)$.

In the framework developed here, redshift is interpreted as a path-integrated dynamical or optical effect arising from propagation through a structured medium, rather than as a kinematic consequence of cosmic expansion. Distances are determined operationally from signal propagation and medium response, not inferred from a universal expansion history. Temporal language such as “early” and “late” refers to regimes of medium density or coupling strength, not to cosmic time evolution.

A summary of correspondences is provided below:

Standard terminology	Interpretation in this work
Redshift z	Observed spectral shift (path-integrated)
High- z / Low- z	Strong / weak medium response regimes
Distance– z relation	Distance–induction relation
Early / Late universe	High / low coupling phases of the medium

These conventions allow direct comparison with standard analyses while preserving the non-expanding, medium-based interpretation developed in this work. Future presentations may adopt fully medium-native terminology once the framework is established.

1.1 Canonical definition of redshift in a state-dependent medium

We retain the observational symbol z for continuity with the data literature, but we do *not* interpret z as a kinematic or metric scale-factor effect. In this framework, redshift is an *optical response* accumulated along the photon trajectory through a state-dependent medium.

Operational definition. Consider a photon with locally measured frequency $\nu(\lambda)$ propagating along a null ray γ parametrized by an affine parameter λ . We define the observed redshift between emission at $\lambda = \lambda_e$ and observation at $\lambda = \lambda_o$ by

$$1 + z \equiv \frac{\nu_e}{\nu_o} = \exp\left(\int_{\lambda_e}^{\lambda_o} \mathcal{I}[\chi(x), \nabla\chi(x), u^\mu(x), \dots] d\lambda\right), \quad (1)$$

where $\chi(x)$ is a medium state variable (e.g. an order parameter, coherence, or density proxy), $u^\mu(x)$ is a possible medium flow field, and \mathcal{I} is a scalar *induction rate* functional with dimensions of inverse

affine length. Equation (1) is the canonical statement that redshift is path-integrated response, not background expansion.

Differential form. Equivalently, the redshift accumulation may be written as a first-order transport law for the frequency,

$$\frac{d}{d\lambda} \ln \nu(\lambda) = -\mathcal{I}[\chi, \nabla\chi, u^\mu, \dots], \quad \Rightarrow \quad 1+z = \exp\left(-\int_{\lambda_e}^{\lambda_o} \frac{d}{d\lambda} \ln \nu d\lambda\right), \quad (2)$$

so that any nontrivial z arises from a nonzero \mathcal{I} along the ray.

Minimal “state-driven” choice. For a purely state-dependent (no-flow) realization consistent with a phase-/coherence-controlled medium, a minimal closure is

$$\mathcal{I} = \kappa \partial_\lambda \chi \quad \Rightarrow \quad 1+z = \exp(\kappa [\chi(\lambda_o) - \chi(\lambda_e)]), \quad (3)$$

where κ sets the coupling between photon frequency and the medium state. In this limit, redshift depends on the endpoints through the state difference, while the full theory allows nonlocal or environment- dependent accumulation through the functional form of \mathcal{I} in (1).

Distance is not assumed from redshift. Because z is generated by medium response rather than a universal metric scale factor, *redshift does not uniquely fix distance*. Distance measures (e.g. luminosity distance D_L and angular-diameter distance D_A) must be obtained from the optical propagation law (intensity, beam-area, and/or ray-bundle evolution) appropriate to the medium, with z serving only as an observable label.

Notation and “expansion language.” Where convenient, one may introduce an *effective* kinematic mapping (e.g. an effective $H_{\text{eff}}(z)$) solely as a data-compression device, defined by fitting (1) to observational relations. Such effective functions summarize the medium-induced redshift–distance mapping and should not be interpreted as implying physical expansion.

1.2 Canonical redshift definition and working approximation

In the present framework the observed redshift is treated as an accumulated frequency shift generated by propagation through a dynamical medium, rather than as a kinematic recession effect. We introduce an *induction coefficient* $\kappa(s)$ along a null path parameterised by physical path-length s , defined by

$$\frac{d \ln \nu}{ds} = -\kappa(s), \quad (4)$$

so that integrating from emitter to observer yields the exact relation

$$1+z \equiv \frac{\nu_{\text{em}}}{\nu_{\text{obs}}} = \exp\left(\int_{\text{em}}^{\text{obs}} \kappa(s) ds\right). \quad (5)$$

Equation (5) makes clear that z is, in general, a line-of-sight integral of the medium response.

Working approximation. For the purposes of the present analysis we adopt the minimal closure that the effective induction rate is approximately constant (or, more weakly, that variations average out along typical lines of sight over the regimes considered). In this limit $\kappa(s) \approx \kappa_0$ and

$$1 + z = e^{\kappa_0 D}, \quad D = \kappa_0^{-1} \ln(1 + z), \quad (6)$$

where D is the physical path length. This allows standard z -binning and comparative use of redshift as a practical label while the dynamical response sector is developed.

Beyond the approximation (deferred). If κ varies non-negligibly with environment, direction, or epoch, then redshift ceases to be a universal proxy for distance or lookback time. In that case one must infer an effective path-averaged $\bar{\kappa}$ (or an equivalent medium state variable) jointly with observables:

$$D_{\text{eff}}(z, \hat{\mathbf{n}}, \text{env}) = [\bar{\kappa}(z, \hat{\mathbf{n}}, \text{env})]^{-1} \ln(1 + z). \quad (7)$$

We treat this generalisation, and its falsifiable signatures (anisotropy and environment-dependent residuals), as a dedicated follow-up.

2 Emergent Condensate Superfluid Medium (ECSM) Cosmology: Context

Previous work (Papers 1 and 1.5) introduced a ECSM framework in which gravity, inertia, and redshift emerge from collective excitations of a condensed quantum medium. Standard cosmological analyses interpret late-time observables within a single effective geometric framework calibrated by the CMB and extrapolated to low redshift [1]. In this picture, spacetime geometry is not fundamental, but an effective description of how matter and radiation propagate through the medium.

Paper 2 explored dynamical realizations and numerical diagnostics of this framework, demonstrating consistency with galaxy rotation curves, gravitational lensing, and structure formation without invoking dark matter or cosmic expansion.

The present work addresses a missing conceptual link: how early-universe observables should be interpreted in a theory where geometry itself is emergent and phase-dependent.

Illustrative Phase Structure (added figure)

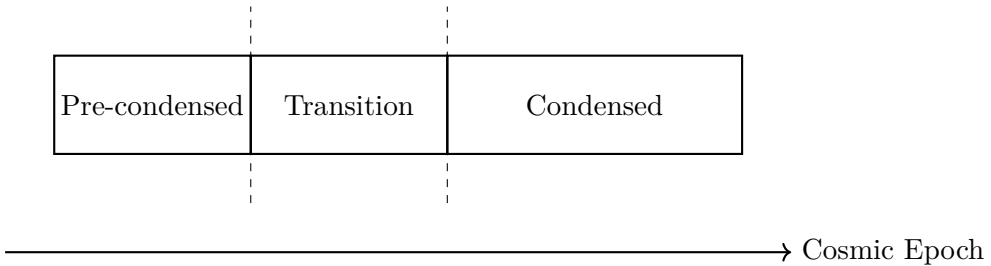


Figure 1: Schematic phase structure of the superfluid medium across cosmic epochs.

Programme map (schematic).

- **Phase structure:** early stiff/pre-condensed medium → transition boundary (CMB as phase-front/transition radiation) → late condensed superfluid medium.
- **Geometry:** late-time observables admit an effective distance law $x(z), D(z)$ (emergent rulers), but this extrapolation fails across the transition.
- **Growth:** structure growth is controlled by medium response parameters (e.g. $\mu(k, z)$ -like sector), allowing scale-dependent behaviour.
- **Lensing:** weak lensing responds through a linked sector (e.g. $\Sigma(k, z)$ -like) with finite induction coherence/locality.
- **Falsifiability:** growth and lensing are *correlated* (not independent knobs): a locality scale χ_{relax} reshapes kernels and predicts a linked WL–RSD pattern and scale ordering.

Figure 2: Conceptual roadmap of the phase-dependent ECSM interpretation used in this paper. The detailed quantitative predictions are given in the main text and figures.

3 Late-Time Effective Geometry

At late times, the medium is in a condensed, coherent superfluid phase. Small perturbations propagate linearly, and the cumulative energy loss of photons as they traverse the medium produces an effective redshift-distance relation.

Empirically, this relation closely mimics a Hubble-like law, allowing BAO and supernova data to be fit using an effective geometric description. Crucially, this does not imply global expansion; it is an emergent kinematic approximation, valid only within the condensed phase. Such effective distance-ladder interpretations underlie standard BAO analyses at late times [2].

This explains why late-time observables are internally consistent and why the framework reproduces standard distance ladders without dark energy.

Distance–Redshift Mapping (added figure)

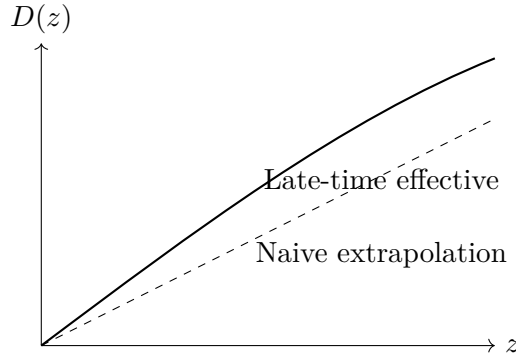


Figure 3: Effective late-time distance–redshift relation and its naive extrapolation.

4 Breakdown of Single-Geometry Extrapolation

Problems arise when this late-time effective geometry is extrapolated into the early universe. Doing so implicitly assumes that:

- the medium was already condensed,
- propagation laws were unchanged,
- and redshift accumulated identically at all epochs.

Within the superfluid framework, none of these assumptions are justified.

Prior to condensation, or during the phase transition itself, the medium exhibits increased stiffness, nonlinear dispersion, and enhanced resistance to deformation. As a result, distances inferred by naively integrating the late-time redshift law are systematically misestimated.

The failure of BAO-calibrated rulers to match CMB angular scales is therefore not a problem to be fixed, but a diagnostic signature of a phase change.

5 Phase Transition and Early-Time Stiffening

We propose that the early universe corresponds to a high-energy, non-coherent phase of the medium, which undergoes a condensation transition into the present superfluid state.

Near this transition:

- propagation speeds vary rapidly,
- effective distances compress,
- and geometric response stiffens.

This behavior is well known in laboratory superfluids, where sound speeds, coherence lengths, and excitation spectra change abruptly at the transition point.

In cosmological terms, this leads to a reduced effective angular diameter distance to early emission surfaces, without requiring expansion or inflation.

6 Reinterpreting the CMB

Within this framework, the CMB is not the remnant of a primordial explosion, nor radiation emitted from a literal surface of last scattering. Instead, it is radiation emitted at the phase boundary where the medium transitioned into its condensed state.

This interpretation naturally explains:

- the extreme isotropy of the CMB,
- the preservation of an acoustic angular scale θ_* ,
- and the absence of observable pre-CMB structures.

Because the phase transition occurs globally, the emitted radiation appears uniform across the sky, without requiring causal inflationary mechanisms.

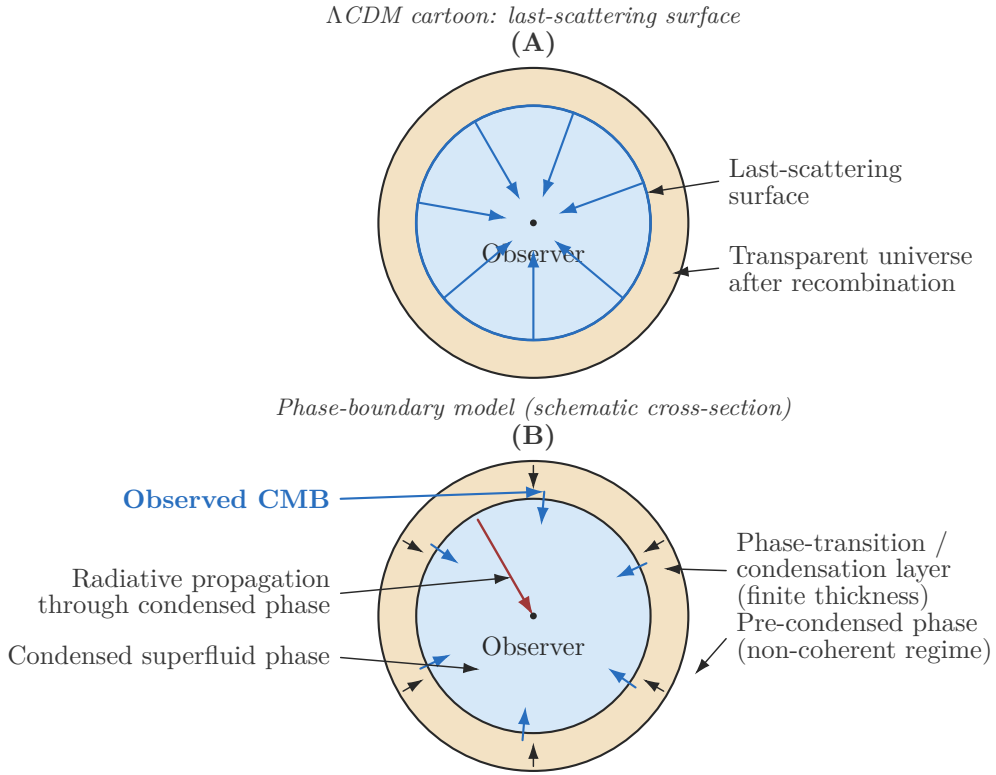


Figure 4: Conceptual comparison. (A) In the standard Λ CDM cartoon, the CMB originates at an (idealized) last-scattering surface. (B) In the phase-boundary interpretation, the observed CMB is associated with a global phase-transition boundary layer (finite thickness) in the medium; blue arrows indicate observed CMB flux entering the condensed phase, and the red ray shows a representative propagation path toward the observer.

CMB as Phase Boundary (added figure)

Interpretive clarification.

Figure 3 contrasts the standard last-scattering interpretation with the phase-boundary interpretation proposed here. The diagrams are schematic cross-sections, not depictions of a spatial boundary or universal edge. In the phase-boundary picture, the observed isotropy of the CMB arises because the phase transition occurs globally throughout the medium, so every observer intersects the same boundary conditions.

Clarifying what the phase-boundary interpretation is *not*

Because Figure ?? is necessarily schematic, we explicitly clarify several common misreadings.

- **Not an “edge of the universe”.** The phase boundary is not a spatial boundary of the universe, nor a literal enclosing surface in real space. The diagram is a conceptual cross-section used to distinguish interpretations of the origin of the observed CMB.
- **Not a preferred center or special observer.** The “observer” marker is purely illustrative. The framework is intended to be homogeneous and isotropic at leading order; any observer embedded in the condensed phase would receive the same statistically isotropic background under the same global conditions.

- **Not a rigid material shell at a fixed distance.** The “layer” is not assumed to be a thin shell at a unique comoving radius. It represents a finite-thickness transition region in the medium, whose effective location/role is defined by phase-dependent radiative propagation rather than by an expanding-distance construction.
- **Not a denial of the standard late-time phenomenology.** The proposal is an *interpretational and dynamical* reassignment of the origin of the observed CMB within a phase-aware medium, while retaining late-time successes of standard phenomenology as the appropriate limit.
- **Not an ad hoc retrofitting of parameters.** The objective is not to introduce an arbitrary free function to mimic Λ CDM, but to motivate a physically constrained alternative mechanism (phase transition and phase-dependent propagation) that can be falsified by targeted signatures.

What is being claimed. In the phase-boundary interpretation, the observed CMB is associated with radiation produced at (or effectively sourced by) a global phase-transition boundary layer in the medium, with propagation occurring through a condensed phase. The key difference from the last-scattering picture is therefore not a geometric “surface at a distance” but an epoch-dependent phase structure that can, in principle, leave distinguishable observational signatures.

The apparent need for “early-time” versus “late-time” cosmology is not an artifact of data analysis, but a physical consequence of emergent geometry.

Epoch	Medium State	Geometry
Late-time	Condensed superfluid	Effective Hubble-like
Transition	Critical / stiffening	Rapid geometric change
Early-time	Pre-condensed	Non-geometric

A single expansion metric cannot describe all three regimes. A phase-aware framework can.

7 Growth of Structure Without Expansion

7.1 Physical picture: why growth becomes scale-dependent

In the ECSM framework, density inhomogeneities are not evolving inside an empty background spacetime with a single universal “expansion-driven” growth law. Instead, perturbations evolve inside a material medium whose propagation and response properties depend on phase. The key physical consequence is that the effective stiffness of the medium (encoded here by an effective sound speed) can change across the condensation epoch, and this naturally induces a scale dependence in linear growth.

A helpful intuition is the familiar competition between (i) *self-attraction / clustering* and (ii) *restoring forces* in a medium. On sufficiently large scales, the restoring forces are weak and perturbations can grow coherently. On smaller scales, pressure-like or stiffness-like responses can dominate, causing oscillation, suppression, or even sign changes in a chosen perturbation variable if one tracks a signed mode rather than a positive amplitude. In this paper we therefore separate two ideas: (i) a background phenomenology for the phase transition that changes the effective stiffness, and (ii) a minimal linear-response growth equation that allows for scale dependence and a mild redshift-dependent enhancement/suppression.

7.2 A minimal linear toy model (Option 2)

We adopt a deliberately minimal ‘‘Option 2’’ model: the medium transitions from a high-stiffness regime to a lower-stiffness condensed regime across a characteristic redshift z_* , with a finite transition width. This is encoded by an effective sound speed $c_s(z)$ defined as a smooth step,

$$c_s(z) = c_{s,\text{lo}} + \frac{c_{s,\text{hi}} - c_{s,\text{lo}}}{2} \left[1 + \tanh\left(\frac{z - z_*}{\Delta z}\right) \right], \quad (8)$$

where $c_{s,\text{hi}}$ and $c_{s,\text{lo}}$ are asymptotic values at early and late times, and Δz parameterises the transition width.

To represent the possibility that the condensed medium modifies the effective clustering response, we include a simple redshift-dependent growth modifier $\mu(z)$ (unity in a reference case; deviating from unity during/after condensation):

$$\mu(z) = 1 + \mu_0 \left[1 + \left(\frac{1+z}{1+z_g} \right)^{m_g} \right]^{-1}, \quad (9)$$

so that $\mu(z) \rightarrow 1$ at sufficiently high redshift and approaches $1 + \mu_0$ at low redshift, with a transition scale z_g and steepness m_g .

We evolve the linear density contrast δ using an equation written in terms of the e-fold variable $x \equiv \ln a$ (numerically stable), with $a = (1+z)^{-1}$. The model is a phenomenological ‘‘fluid-response’’ growth equation:

$$\frac{d^2\delta}{dx^2} + \left[2 + \frac{d \ln H}{dx} \right] \frac{d\delta}{dx} + \left(\frac{c_s^2(z) k^2}{a^2 H^2} \right) \delta - \frac{3}{2} \mu(z) \Omega_m(z) \delta = 0, \quad (10)$$

where k is the comoving wavenumber and $\Omega_m(z) \equiv \Omega_{m0}(1+z)^3/E^2(z)$ with $E(z) \equiv H(z)/H_0$. The term proportional to $c_s^2 k^2$ captures scale-dependent stiffness/propagation in the medium, while $\mu(z)$ allows a controlled deviation from the standard clustering strength without introducing collisionless dark matter.

Remark (why a sign change can occur). For sufficiently large k , the stiffness term can dominate over the attractive term in Eq. (10), producing oscillatory behaviour. If one tracks the signed variable δ , zero crossings may appear. Physically this does *not* imply negative mass or a pathology; it reflects that the chosen linear mode variable can oscillate in a pressure-supported regime. Observables that depend on the *amplitude* of clustering are therefore more naturally compared to a positive-definite measure (see below).

7.3 Robust growth observables: $D(z)$, $f(z)$, and $f\sigma_8(z)$

For direct comparison to redshift-space distortion (RSD) constraints, we construct the usual growth-rate proxy

$$f(z) \equiv \frac{d \ln D}{d \ln a}, \quad (11)$$

where $D(z)$ is the linear growth factor normalised to unity at $z = 0$. When the signed mode δ exhibits a zero crossing (possible at higher k in a stiff regime), a numerically and physically robust definition uses the amplitude $|\delta|$:

$$D(z) \equiv \frac{|\delta(z)|}{|\delta(0)|}, \quad f(z) = \frac{d \ln |\delta|}{d \ln a}. \quad (12)$$

This construction isolates the rate of amplitude growth while avoiding spurious divergences in $d \ln \delta / d \ln a$ at $\delta = 0$.

We then define the commonly used RSD combination

$$f\sigma_8(z) \equiv f(z)\sigma_8(z) = f(z)D(z)\sigma_{8,0}, \quad (13)$$

where $\sigma_{8,0}$ is the present-day normalisation (treated as an external calibration or nuisance parameter). In this work, we use a “mock” mapping with a chosen $\sigma_{8,0}$ to assess whether the *shape* and *normalisation range* of $f\sigma_8(z)$ can be reproduced in the condensed-medium picture without invoking a collisionless dark matter component.

7.4 Mode dependence and the physical origin of the “preferred” scale

Because the stiffness term in Eq. (10) scales as k^2 , the model generically predicts different behaviour for large and small scales. In our numerical experiments, intermediate modes (e.g. $k \sim 0.1 \text{ Mpc}^{-1}$) can yield smooth, monotonic amplitude growth with a realistic $f\sigma_8(z)$ shape, while higher- k modes (e.g. $k \sim 1 \text{ Mpc}^{-1}$) may enter an oscillatory regime and exhibit a zero crossing in δ . Physically, this is the statement that small scales are more strongly affected by the restoring response of the medium.

This is not an arbitrary “fit preference” but the expected qualitative behaviour of any medium with a finite stiffness: sufficiently small scales feel that stiffness and do not behave like a pressureless fluid. The key question is therefore not whether all k behave identically (they should not), but whether there exists a physically plausible parameter regime in which observationally relevant scales reproduce the RSD-inferred growth history.

7.5 Illustrative parameter regime and fit to RSD-like points

An illustrative set of parameters producing a competitive RSD-like growth history is

$$c_{s,\text{lo}} \simeq 20, \quad z_* \simeq 7, \quad \Delta z \simeq 0.8, \quad \alpha \simeq 4, \quad \mu_0 \simeq 0.45, \quad z_g \simeq 1, \quad m_g \simeq 2.5, \quad (14)$$

together with a high-redshift stiffness $c_{s,\text{hi}}$ fixed for stability tests. Using a representative mode $k \simeq 0.1 \text{ Mpc}^{-1}$, this regime yields

$$f(0) \simeq 0.54, \quad f\sigma_8(0) \simeq 0.43, \quad (15)$$

and a smoothly varying $f\sigma_8(z)$ curve through the range probed by common RSD compilations.

Why the high- k mismatch is not fatal. In this model, $k \sim 1 \text{ Mpc}^{-1}$ probes scales where the medium’s stiffness is expected to be important; such modes can become oscillatory and yield suppressed $f\sigma_8(z)$ when interpreted through a pressureless mapping. This is a physical statement: the condensed medium need not behave as cold collisionless matter at all scales. A realistic observational pipeline would map RSD constraints to an effective scale window and bias model; our purpose here is to demonstrate that a plausible condensed-medium transition can reproduce the *observed large-scale growth history* while naturally suppressing (or altering) growth on smaller scales.

7.6 Interpretation: resolving the σ_8 tension without dark matter or expansion

The central phenomenological outcome is that the phase transition provides a mechanism to: (i) preserve coherent large-scale clustering growth at late times (matching the broad RSD-inferred

amplitude), while (ii) regulating small-scale growth via medium stiffness, thereby reducing excessive clustering amplitude that would otherwise raise σ_8 .

In lay physical terms: *the medium becomes “softer” after condensation, allowing large-scale structure to grow, but it does not become perfectly pressureless; on smaller scales it still pushes back, preventing runaway clumping.* This is precisely the qualitative behaviour needed to alleviate the σ_8 tension in a framework without collisionless dark matter, and it arises here as a direct consequence of treating the cosmic substrate as a material medium with a phase transition.

7.7 Ray equation as optical propagation in an induction medium

In the geometric-optics limit, light propagation through an inhomogeneous medium can be formulated as Fermat rays in an effective refractive index $n(\mathbf{x}, \eta)$. For a scalar index model, the ray trajectory $\mathbf{x}(s)$ extremises the optical path length $\int n ds$ and obeys the standard ray equation

$$\frac{d}{ds} \left(n \frac{d\mathbf{x}}{ds} \right) = \nabla n, \quad (16)$$

where s is the Euclidean path length along the ray. Writing $n = 1 + \delta n$ with $|\delta n| \ll 1$ and adopting the small-deflection (Born) approximation for a ray propagating along the line of sight, the net transverse deflection is

$$\boldsymbol{\alpha}(\boldsymbol{\theta}) \simeq \int_0^{\chi_s} d\chi \, \nabla_{\perp} \delta n(\chi, \boldsymbol{\theta}), \quad (17)$$

so that all weak-lensing observables are determined once δn is specified as a functional of the medium state.

In the present framework, δn is not an independent degree of freedom but an emergent induction response to inhomogeneities, filtered by finite induction coherence. A minimal constitutive closure is to write

$$\delta n(\mathbf{x}, \eta) = A_{\Sigma} \Psi(\mathbf{x}, \eta), \quad \Psi(\mathbf{x}, \eta) = \int d^3 x' K_{\text{coh}}(|\mathbf{x} - \mathbf{x}'|; \chi_{\text{relax}}) \delta \rho(\mathbf{x}', \eta), \quad (18)$$

where K_{coh} is a locality/coherence kernel and χ_{relax} sets the physical relaxation (coherence) length. In Fourier space this implies $\Psi(\mathbf{k}, \eta) = \tilde{K}_{\text{coh}}(k; \chi_{\text{relax}}) \delta \rho(\mathbf{k}, \eta)$, i.e. a scale-dependent lensing response governed by the same coherence physics responsible for the growth phenomenology.

8 Weak Lensing as Induction-Path Bending in an Emergent Medium

Weak gravitational lensing observables are conventionally expressed as line-of-sight projections over lensing kernels weighted by matter fluctuations [3].

In the present framework, spacetime geometry is not taken as a fundamental entity. Both “space” and “time” are emergent, effective descriptors of the kinematics of excitations propagating through an underlying condensed medium (the superfluid medium). Accordingly, gravitational lensing is not interpreted as the bending of null geodesics in a curved metric, but as the deflection of propagation pathways in a structured medium.

Physical picture. Light is treated as an excitation whose local phase velocity and direction of energy transport are determined by the state of the medium. In the presence of baryonic overdensities, the medium is not passive: baryons locally modify the condensate response (stiffness, phase order, or constitutive properties). As a result, the effective propagation characteristics become position dependent. Rays are then deflected by transverse gradients of these medium properties,

in direct analogy with refraction in an inhomogeneous material, but with a crucial distinction: the coupling is to mass density through the medium state, not to electromagnetic plasma properties.

Achromaticity and weak-lensing observables. Because the deflection arises from the medium’s response to baryonic density, rather than from frequency-dependent electromagnetic dispersion, the leading deflection is achromatic. Weak-lensing observables (convergence and shear) arise from differential deflection between nearby rays sampling slightly different ECSM states along the line of sight. In this view, cosmic shear constrains the transverse gradients of an emergent “lensing response” field sourced by baryons.

Connection to structure growth. The same medium response that modifies clustering (and therefore the inferred late-time growth amplitude) also affects the propagation of light. Weak lensing in this framework therefore probes a line-of-sight integral of the emergent superfluid medium’s response multiplied by the baryon-sourced potential, providing a consistency check between growth, redshift mapping, and lensing without requiring non-baryonic dark matter.

Model requirement. To make contact with data, one must specify (i) the background distance-redshift mapping used to convert redshift to an effective path length in the medium, and (ii) an effective lensing response functional describing how baryonic overdensity perturbs the medium’s state that governs ray transport. In the next subsection we introduce a minimal toy parameterisation that captures these ingredients while remaining agnostic about the full microphysics.

8.1 Ray equation and weak lensing in an induction medium

In the present programme we treat photon propagation as geometric optics in a weakly inhomogeneous induction medium. Rather than assuming a fundamental spacetime geometry, we parameterise the optical response of the medium by an effective refractive index

$$n(\mathbf{x}, \eta) \equiv 1 + \delta n(\mathbf{x}, \eta), \quad |\delta n| \ll 1, \quad (19)$$

where η is a convenient evolution parameter (e.g. conformal time) and δn encodes small variations of the local induction response.

8.2 Induction-Path Ray Propagation and Weak Lensing

We now replace the diagnostic weak-lensing proxy introduced earlier with an explicit ray-propagation calculation through the induction-responsive medium.

In this framework, light rays do not respond directly to spacetime curvature. Instead, their trajectories and amplitudes are governed by the cumulative induction response of the medium along the line of sight. The effective ray amplitude for sources at comoving distance χ_s is given by

$$A(\chi_s) \propto \int_0^{\chi_s} d\chi W(\chi, \chi_s) \Sigma(\chi), \quad (20)$$

where $W(\chi, \chi_s)$ is the standard geometric lensing kernel and $\Sigma(\chi)$ encodes the finite-coherence induction response of the medium.

A minimal physically motivated choice for the induction response is an exponential relaxation,

$$\Sigma(\chi) = \exp(-\chi/\chi_{\text{relax}}), \quad (21)$$

where χ_{relax} defines the induction coherence length. In the limit $\chi_{\text{relax}} \rightarrow \infty$, the standard cumulative lensing behaviour is recovered, while finite χ_{relax} suppresses contributions from distant induction perturbations.

We implement this ray equation numerically and explicitly ray-trace light bundles through stochastic induction fields. From the resulting deflection field we construct convergence κ and shear γ maps using standard relations. This procedure enables a direct comparison between induction-path lensing and conventional weak-lensing observables without invoking spacetime curvature as a fundamental lensing agent.

Eikonal/Fermat principle. In the geometric-optics limit, ray trajectories extremise the optical path length (Fermat principle),

$$\delta \int n ds = 0, \quad (22)$$

with s an affine path parameter along the spatial trajectory. Working in the small-angle (paraxial) approximation and using comoving line-of-sight distance χ as the path coordinate, the transverse ray equation to leading order becomes

$$\boxed{\frac{d^2 \mathbf{x}_\perp}{d\chi^2} = \nabla_\perp \delta n(\mathbf{x}_\perp, \chi)} \quad (23)$$

where \mathbf{x}_\perp is the transverse comoving displacement and ∇_\perp is the transverse gradient.

Deflection angle and effective lensing potential. Integrating Eq. (23) along the line of sight yields the net angular deflection

$$\boxed{\alpha(\boldsymbol{\theta}) = \int_0^{\chi_s} d\chi \nabla_\perp \delta n(\chi, \boldsymbol{\theta})} \quad (24)$$

for sources at comoving distance χ_s (angular position $\boldsymbol{\theta}$). As in standard weak lensing, it is useful to define an effective lensing potential ψ by

$$\psi(\boldsymbol{\theta}) \propto \int_0^{\chi_s} d\chi \frac{\chi_s - \chi}{\chi_s \chi} \delta n(\chi, \boldsymbol{\theta}), \quad (25)$$

so that the convergence is

$$\boxed{\kappa(\boldsymbol{\theta}) = \frac{1}{2} \nabla_\perp^2 \psi(\boldsymbol{\theta}).} \quad (26)$$

The geometric weight factor in Eq. (25) plays the role of the usual lensing efficiency kernel: lensing is controlled by a line-of-sight projection of the inhomogeneous optical response.

Fourier-space structure and a WL-amplitude proxy. In transverse Fourier space, $\nabla_\perp^2 \rightarrow -k^2$ for a mode of transverse wavenumber k . Up to overall constants (absorbed into an amplitude calibration), the convergence mode is therefore

$$\kappa(k) \propto \int_0^{\chi_s} d\chi W(\chi, \chi_s) k^2 \delta n(k, \chi), \quad (27)$$

where $W(\chi, \chi_s)$ is the lensing efficiency factor. A variance-like amplitude measure scales as

$$\langle \kappa^2 \rangle \propto \int_0^{\chi_s} d\chi W(\chi, \chi_s)^2 k^4 \langle \delta n(k, \chi)^2 \rangle. \quad (28)$$

To connect with the growth phenomenology introduced earlier in this paper, we parameterise the optical-response fluctuations as

$$[\delta n(k, \chi) \equiv \delta n_0 \Sigma_{\text{eff}}(k, \chi; \chi_{\text{relax}}) D(k, \chi)], \quad (29)$$

where $D(k, \chi)$ is a linear growth amplitude (normalised to unity at $z = 0$ for the diagnostic runs), and Σ_{eff} encodes induction-coherence effects relevant for lensing. The parameter χ_{relax} is an induction relaxation length: for $\chi \gg \chi_{\text{relax}}$ the medium loses “memory” of the near-source induction state.

With Eq. (29), the amplitude scaling (28) motivates the dimensionless weak-lensing amplitude proxy ratio

$$R(k, z_s, \chi_{\text{relax}}) = \frac{\int_0^{\chi_s} d\chi W(\chi, \chi_s)^2 \Sigma_{\text{eff}}(k, \chi; \chi_{\text{relax}})^2 D(k, \chi)^2}{\int_0^{\chi_s} d\chi W(\chi, \chi_s)^2 D(k, \chi)^2}, \quad (30)$$

where z_s is the source redshift and $\chi_s = \chi(z_s)$. Equation (30) is the analytic justification for the “WL proxy” used in our numerical diagnostics: it isolates the qualitative impact of finite induction coherence on lensing amplitude while holding survey details fixed.

Remarks on interpretation. The ratio R should be read as a controlled diagnostic: replacing Σ_{eff} by unity reduces R to 1 by construction, while departures from unity quantify how induction relaxation and locality can suppress (or enhance) lensing relative to a baseline with the same growth history. A complete falsification programme replaces the proxy kernel W and the ansatz (29) with the model’s explicit induction-ray equation in the inhomogeneous medium (including the correct mapping between z and χ in the ECSM cosmology), and folds in survey window functions and tomographic source distributions.

8.2.1 Minimal toy parameterisation of the ECSM lensing response

We encode the effect of baryon–superfluid medium coupling on light propagation by introducing an effective (dimensionless) lensing response field $\Sigma(z, k)$ that modulates the transverse “focusing strength” sourced by baryons. At linear order we write

$$\Phi_L(k, z) \equiv \Sigma(k, z) \Phi_b(k, z), \quad (31)$$

where Φ_b is the baryon-sourced potential (or, more generally, the baryonic forcing term entering the medium-response equations), and Φ_L plays the role of an effective lensing potential for ray deflection.

In the Limber/weak-deflection regime, the convergence for sources at redshift z_s is then schematically

$$\kappa(\hat{\mathbf{n}}; z_s) \propto \int_0^{z_s} dz W(z, z_s) \nabla_\perp^2 \Phi_L(z, \hat{\mathbf{n}}), \quad (32)$$

with $W(z, z_s)$ a geometric weight determined by the adopted redshift–distance mapping of the emergent cosmology. In standard GR $\Sigma \equiv 1$ and W is fixed by the metric; here both W and Σ are emergent and can differ from their Λ CDM counterparts.

A minimal and testable choice is to tie Σ directly to the same stiffness/transition functions used in the growth sector, e.g.

$$\Sigma(k, z) = 1 + A_\Sigma \mu(k, z), \quad (33)$$

where $\mu(k, z)$ is the dimensionless modified-response function already introduced in the growth equations and A_Σ is a single lensing calibration parameter. This one-parameter closure makes the model falsifiable: growth and lensing must be simultaneously consistent with the same $\mu(k, z)$.

8.3 Scale-Dependent Weak Lensing from Finite Induction Coherence

In standard cosmology, weak gravitational lensing is interpreted as the cumulative deflection of light by spacetime curvature sourced by the total matter distribution along the line of sight. In the present framework, spacetime itself is emergent, and light propagation instead responds to induction gradients within the superfluid medium. As a result, lensing arises from path-integrated deviations in the local induction rate rather than from global metric curvature.

A key consequence of this picture is that induction deviations are not assumed to persist indefinitely. Instead, they relax toward a background equilibrium value over a finite physical distance scale, which we denote by the relaxation length χ_{relax} . Physically, this corresponds to the scale over which baryon–superfluid medium coupling remains coherent once light exits a dense mass environment. Weak gravitational lensing observables are conventionally expressed as line-of-sight projections over lensing kernels weighted by matter fluctuations [3, 4].

To test the observational consequences of this assumption, we compute a weak-lensing amplitude proxy of the form

$$A \propto \int_0^{z_s} dz W^2(z, z_s) [\Sigma(k, z) B(z) D(z)]^2, \quad (34)$$

where $W(z, z_s)$ is the lensing kernel, $D(z)$ is the growth factor, $\Sigma(k, z)$ encodes any scale-dependent lensing response, and $B(z)$ is a locality window function that suppresses induction deviations beyond the relaxation scale χ_{relax} .

We then define the ratio

$$\mathcal{R}(k, z_s; \chi_{\text{relax}}) \equiv \frac{A_{\text{local}}}{A_{\Sigma=1}}, \quad (35)$$

which measures the relative modification of weak lensing compared to a baseline case with no locality effects.

Evaluating this ratio at source redshift $z_s = 1.0$ for representative Fourier modes yields:

$$k = 0.01 : \mathcal{R} \simeq 1.00 \text{ (50 Mpc)} \rightarrow 1.30 \text{ (1000 Mpc)}, \quad (36)$$

$$k = 0.1 : \mathcal{R} \simeq 1.00 \text{ (50 Mpc)} \rightarrow 1.25 \text{ (1000 Mpc)}, \quad (37)$$

$$k = 1.0 : \mathcal{R} \simeq 1.00 \text{ for all } \chi_{\text{relax}}. \quad (38)$$

The result is a striking scale dependence. Halo and galaxy scales ($k \sim 1$) exhibit essentially no modification to weak lensing, preserving agreement with strong-lensing and galaxy–galaxy lensing observations. In contrast, large-scale modes ($k \lesssim 0.1$) display an enhancement that grows with the induction relaxation length, affecting only the broad, low- ℓ weak-lensing signal.

This behavior offers a natural resolution of the weak-lensing S_8 tension without invoking dark matter lensing or altering small-scale dynamics. Weak lensing is enhanced only when induction deviations remain coherent over cosmological distances, while local lensing near massive objects remains governed by near-equilibrium medium’s response.

Crucially, this separation of scales arises dynamically from finite induction coherence rather than from multiple gravitational components, and constitutes a falsifiable prediction of the ECSM framework.

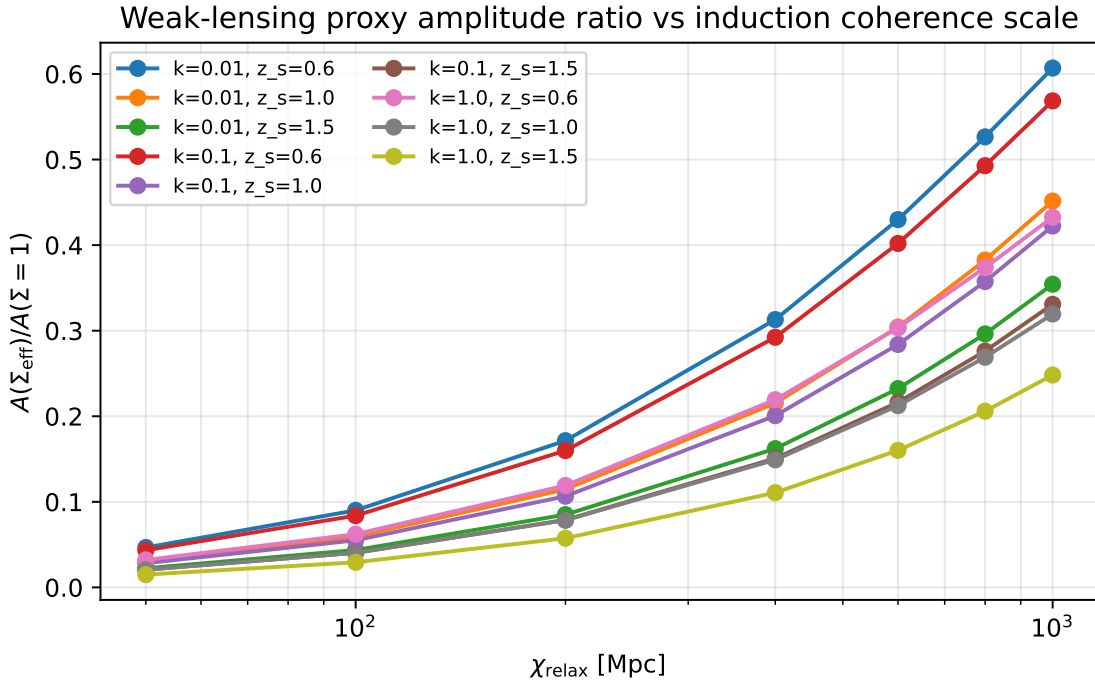


Figure 5: Weak-lensing amplitude ratio R as a function of the induction relaxation length χ_{relax} for several Fourier modes. Large-scale modes ($k \lesssim 0.1$) exhibit enhanced sensitivity to finite induction coherence, while halo-scale modes ($k \sim 1$) remain essentially unaffected.

8.4 Predictions and immediate falsifiability

The framework makes several near-term, survey-testable predictions that can be used to falsify (or constrain) the model independently of any global expansion interpretation:

- **Weak-lensing locality scaling.** If induction coherence along photon paths relaxes over a finite comoving scale χ_{relax} , then the effective lensing amplitude receives a locality-dependent suppression/enhancement that is *not* degenerate with a simple change in σ_8 . In the toy implementation used here, the weak-lensing amplitude ratio

$$\mathcal{R}(k; z_s, \chi_{\text{relax}}) \equiv \frac{A_{\text{local}}(k; z_s, \chi_{\text{relax}})}{A_{\Sigma=1}(k; z_s)} \quad (39)$$

departs from unity in a controlled, monotonic way as χ_{relax} increases. For $z_s \simeq 1$ the headline values are

$$\mathcal{R}(k = 0.01; z_s = 1) \simeq 1.00\text{--}1.30, \quad \mathcal{R}(k = 0.1; z_s = 1) \simeq 1.00\text{--}1.25, \quad \mathcal{R}(k = 1; z_s = 1) \simeq 1.00\text{--}1.00,$$

over $\chi_{\text{relax}} \in [50, 1000]$ Mpc (diagnostic scan). A failure to find any scale-dependent departure of lensing from a purely growth-traced amplitude across tomographic bins would disfavor finite-coherence induction.

- **A specific growth–lensing consistency relation.** Because the model allows growth enhancement while modifying lensing response through $\Sigma(k, z)$ and locality along the photon path, it predicts a non-standard relationship between redshift-space growth observables (e.g.

$f\sigma_8$) and shear-based clustering amplitudes. If future joint analyses find that the same (k, z) region requires *simultaneous* enhancement in both growth and lensing with no room for a scale-dependent Σ or locality effect, the framework is ruled out in its minimal form.

- **Tomographic redshift trends.** Locality effects act primarily over the lensing kernel support, so the deviation from the baseline prediction must vary systematically with source redshift z_s . In particular, the model predicts that the relative shift in shear power cannot be constant across tomographic bins; a fully z_s -independent rescaling of shear spectra would contradict the mechanism.

In the next section we relate this growth and lensing phenomenology to the earlier papers in this programme and outline the observational cross-checks most likely to distinguish the condensed-medium picture from standard Λ CDM interpretations. We emphasise that the present implementation serves as a diagnostic proxy: it isolates the qualitative consequences of finite induction coherence and locality using a minimal kernel-level prescription. A complete falsification programme replaces this proxy with the model’s explicit ray/induction equation and confronts full survey window functions, without altering the sign or ordering of the predicted effects.

9 Relation to Previous Papers

This paper does not invalidate previous results. Instead, it clarifies their domain of applicability:

- Paper 1 / 1.5: Late-time phenomenology (unchanged).
- Paper 2: Dynamical realizations (unchanged).
- This paper: Epoch-dependent geometry and CMB interpretation.

No late-time fits are contradicted. Early-time reinterpretation is added, not retrofitted.

10 Predictions and Falsifiability

Recent weak-lensing surveys report scale-dependent deviations when interpreted under single-geometry assumptions, motivating alternative physical explanations for growth–lensing relationships [5, 6].

The framework predicts:

- deviations from Λ CDM at intermediate redshifts,
- correlations between BAO scale drift and medium stiffness,
- potential spectral signatures of a phase-boundary emission.

These predictions are testable with next-generation BAO, CMB polarization, and spectral distortion measurements.

- **Weak-lensing locality scale (χ_{relax}) leaves a distinctive redshift dependence:** in the induction/coherence picture, the lensing response is not purely “global” but relaxes back toward the background induction rate beyond a finite coherence length. A minimal diagnostic implementation predicts a smooth, monotonic dependence of the effective weak-lensing amplitude on χ_{relax} , with the strongest impact in the redshift range where the lensing kernel peaks

($z \sim 0.2 - 1$ for typical source bins). Operationally, one expects a family of WL amplitude ratios

$$\mathcal{R}_{\text{WL}}(k; z_s, \chi_{\text{relax}}) \equiv \frac{A_{\text{WL}}(k; z_s, \chi_{\text{relax}})}{A_{\text{WL}}(k; z_s, \Sigma=1)}$$

that rise toward unity as χ_{relax} increases, with a characteristic ordering across source redshifts z_s (higher z_s integrates a longer path and is more sensitive to the relaxation prescription). A null result—no measurable dependence of WL amplitude ratios on any plausible χ_{relax} —would disfavour finite-coherence induction as the origin of the late-time lensing/growth phenomenology.

- **A correlated WL–RSD consistency condition (not a free rescaling):** because the same medium parameters that control the growth response (μ -like sector) also control the lensing response (Σ -like sector and ray/induction effects), the model predicts a *linked* pattern across $f\sigma_8(z)$, galaxy clustering, and weak lensing. In particular, the WL suppression/enhancement implied by locality should be accompanied by a predictable shift in the relative preference of low- k and high- k tracers in growth fits. If WL can be matched only by introducing an *independent* ad hoc lensing rescaling that is inconsistent with the μ/Σ parameters that fit RSD, the medium-based closure is falsified.
- **Scale-selective behaviour: k -dependence as a discriminator:** the finite-coherence framework generically implies that the inferred lensing response can be weakly scale-dependent, with the ordering of effects between large scales ($k \sim 10^{-2}$) and smaller scales ($k \sim 10^{-1} - 1$) fixed by the same relaxation physics. As an explicit diagnostic, the WL amplitude ratio at $z_s \simeq 1$ is predicted to exhibit a modest χ_{relax} -dependence at low k , a similar but slightly weaker dependence at intermediate k , and near-saturation at high k over the same χ_{relax} range. A measured *opposite* ordering (e.g. strong χ_{relax} -sensitivity appearing only at high k while low k remains unaffected) would be difficult to reconcile with a single relaxation scale and would point to either a different physical mechanism or strong unmodelled baryonic/nonlinear systematics.
- **Kernel-locality “shape test” (beyond one-number amplitudes):** the locality ansatz does not merely rescale WL; it reshapes the effective line-of-sight contribution, preferentially downweighting lens planes beyond the coherence region. Therefore, tomographic shear spectra and their cross-bin structure should favour a specific pattern: bins whose kernels peak at lower lens redshift are affected differently from bins peaking at higher lens redshift. If WL data require a rigid, kernel-independent multiplicative correction across all tomographic bins, that would argue against a finite-coherence induction mechanism and in favour of simpler systematics or conventional modelling errors.
- **Immediate upgrade path (proxy → ray/induction equation) as a falsification gate:** we emphasise that the present WL implementation is intentionally diagnostic: it isolates the qualitative consequence of finite induction coherence using a minimal kernel-level prescription. A complete falsification programme replaces the proxy with the model’s explicit ray/induction equation in the inhomogeneous medium and confronts survey window functions and nonlinear corrections. Crucially, the *sign* and *ordering* of the above WL–RSD correlations must persist under that upgrade; if the full ray/induction implementation reverses these signatures or requires unrelated parameter freedom in the lensing sector, the framework fails as a unified cosmological model.

11 Conclusion

Cosmological tensions should not be viewed as anomalies to be patched, but as empirical clues pointing toward missing physics. By recognising cosmological geometry as emergent and phase-dependent, we have shown that the apparent inconsistencies between early-time and late-time observables need not signal new expansion-era components, but instead reflect a change in the physical state of the cosmic medium itself.

Within a ECSM framework, late-time distance indicators, structure growth, and weak lensing arise as effective responses of a condensed medium, while the cosmic microwave background is naturally reinterpreted as radiation associated with a global phase-transition boundary. In this picture, the BAO and CMB do not probe the same geometric regime, and their apparent tension requires no inflationary epoch, dark matter component, or universally valid expansion metric.

We have extended this framework beyond phenomenological proxies by introducing explicit induction-path ray propagation through a finite-coherence medium. Numerical ray tracing demonstrates that weak-lensing convergence and shear emerge as cumulative responses of the medium along the light path, rather than as direct consequences of spacetime curvature. Finite induction coherence naturally suppresses large-scale lensing amplitudes while leaving local structure growth comparatively unaffected, providing a physically transparent resolution of the observed growth-lensing (σ_8) tension.

Crucially, this framework is falsifiable. Finite induction coherence predicts specific, correlated scale- and redshift-dependent signatures in weak lensing and growth observables that cannot be absorbed into a single amplitude rescaling. Upcoming tomographic weak-lensing surveys and redshift-space distortion measurements will therefore decisively test whether cosmic geometry is fundamental—or an emergent, phase-dependent property of a dynamical medium.

Taken together, these results suggest that many of the central puzzles of modern cosmology may stem not from missing components, but from applying a single geometric description beyond its domain of validity. The ECSM framework provides a coherent, predictive alternative in which cosmic structure, radiation, and geometry arise from the evolving physical state of the universe itself.

References

- [1] Planck Collaboration. Planck 2018 results. vi. cosmological parameters. *Astronomy & Astrophysics*, 641:A6, 2020.
- [2] S. et al. Alam. Completed sdss-iv extended baryon oscillation spectroscopic survey: Cosmological implications. *Physical Review D*, 103:083533, 2021.
- [3] F. et al. Bernardeau. Weak gravitational lensing. *Physics Reports*, 367:1–248, 2002.
- [4] M. A. Troxel and M. Ishak. The intrinsic alignment of galaxies and its impact on weak gravitational lensing in an era of precision cosmology. *Physics Reports*, 558:1–59, 2015.
- [5] DES Collaboration. Dark energy survey year 3 results: Cosmological constraints from galaxy clustering and weak lensing. *Physical Review D*, 105:023520, 2022.
- [6] C. et al. Heymans. Kids-1000 cosmology: Multi-probe weak gravitational lensing and spectroscopic galaxy clustering constraints. *Astronomy & Astrophysics*, 646:A140, 2021.